Supporting Information

Halbach Effect at the Nanoscale from Chiral Spin Textures

Miguel A. Marioni[1,*], Marcos Penedo[1], Mirko Baćani[1], Johannes Schwenk[1,2], Hans J. Hug[1,3]

[1] **Empa, Swiss Federal Laboratories for Materials Science and Technology, CH-8600 Dübendorf, Switzerland.**

[2] **Center for Nanoscale Science and Technology, National Institute of Standards and Technology, Gaithersburg, MD 20899, United States.**

[3] **Department of Physics, University of Basel, CH-4056 Basel, Switzerland.**

E-mail: miguel.marioni@empa.ch

Quantitative measurements by Magnetic Force Microscopy (MFM)

Contrast formation in the MFM ideally is the result from the interaction of an extended magnetic tip with the stray field gradients of the sample. For convenience the process is described in coordinates $\boldsymbol{k} = (k_x, k_y)$ of the 2D reciprocal-space for the scan plane, and direct space for the tip-sample distance z along the scan plane normal. It can be shown[1] that the MFM signal $\Delta f(\boldsymbol{k}, z)$ measured at tip-sample distance z for a stray field $H_z(\boldsymbol{k}, z)$ depends on the instrument calibration function $ICF(\boldsymbol{k}, z)$ as

$$\Delta f(\boldsymbol{k}, z) = ICF(\boldsymbol{k}, z)\,\frac{dH_z}{dz}(\boldsymbol{k}, z) \tag{1}$$

The $ICF(\boldsymbol{k}, z)$ includes terms for the geometry and orientation of the cantilever, as well as its mechanical and magnetic properties. Importantly, it includes the information on the distribution in space of the magnetic charges of the MFM tip.

Calibrating the instrument or the tip is essentially an inversion of Equation (1). We determine the $ICF(\boldsymbol{k}, z)$ from 2601 MFM scans of domains with narrow-wall through-thickness perpendicular domains from a $(Co_{0.6nm}/Pt_{1.0nm})_{\times 5}$ thin film multilayer. All MFM Δf-

images have been acquired at the same tip-sample distance of 12 nm, with maximum departures of ±0.5 nm. Recall that stray fields of a thin film samples are subject to so-called distance losses[2,3], which describe a rapid decrease with distance of the field amplitude for high spatial frequencies in the field (exponential factors of $-k \cdot z$). The ensuing unequal degradation of the SNR for high and low spatial frequencies is a practical restriction of the usefulness of Eq. (1) for high frequencies, i.e. small magnetic features. A further evident difficulty connected to distance losses is that the measured amplitudes vary strongly with distance, so that maintaining stability of the scan plane is essential. We utilize a distance $z = 12$ nm that ensures a useful SNR for wavelengths as small as 20 nm and still ensures a moderately small signal from the sample topography, when scanning at constant average height. For tip-sample distance control we rely on capacitive excitation of the second flexural cantilever oscillation mode [4]. With this the tip-sample distance can be kept constant within to ±0.5 nm over several hours.

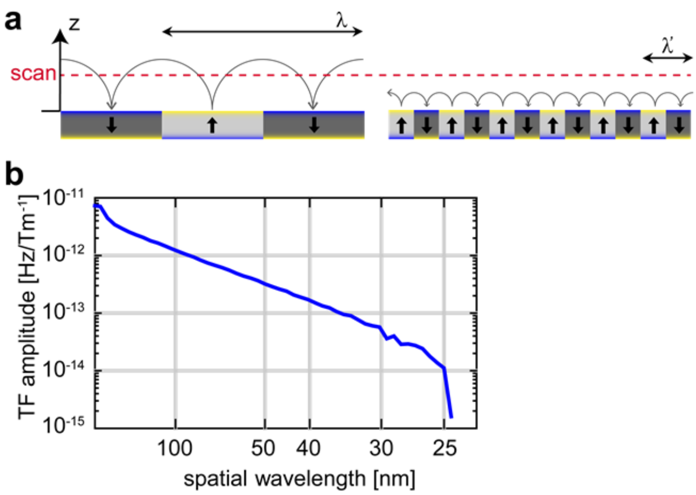

Figure 1: Distance loss and calibration function. a Schematic of the stray fields from magnetic domain structures with characteristic features of different wavelength. Stray fields from wider (λ) features' penetrate deeper into space than stray fields from narrow features λ. **b** Sensitivity of the tip for different spatial wavelengths of the z-derivative of the z-component of the magnetic stray field.

Stray field components

Because the MFM scans a space devoid of sources of magnetic field, in practice we can write the latter as the gradient of a magnetic potential, $\mathbf{H}(\mathbf{r}) = -\nabla\phi_m(\mathbf{r})$, where ϕ_m satisfies the Laplace equation. For definiteness we assume the sources of the stray field (provided by the sample) are described by a boundary condition on the xy plane, parallel to the scan plane located at distance z from the boundary. In the 2D Fourier space utilized in the previous section, this leads to the convenient expression

$$\mathbf{H}(\mathbf{k}, z) = (\mathrm{i}k_x, \mathrm{i}k_x, -k)\phi_m(\mathbf{k}, z), \tag{2}$$

and therefore also to

$$\mathbf{H}(\mathbf{k}, z) = (-\mathrm{i}\frac{k_x}{k}, -\mathrm{i}\frac{k_y}{k}, 1)H_z(\mathbf{k}, z). \tag{3}$$

Consequently, the measurement of the z-component of the stray field provides the remaining components as well, and implies that if $ICF(\mathbf{k}, z)$ is known the MFM can measure the stray field vector.

Field from a given magnetization pattern

For a thin film extending on the xy plane and perpendicular to if from $z =- d$ to $z = 0$ and with through-thickness homogeneous magnetization, the stray field for $z > 0$ can be written:

$$H_z(\mathbf{k}, z) = \frac{1}{2}\,(1 - e^{-kd})e^{-kz}\,\left(\sigma(\mathbf{k})\,+\frac{\rho(\mathbf{k})}{k}\right) \tag{4}$$

where the factors e^{-kz} and $(1 - e^{-kd})$ are the distance- and thickness-loss factors, respectively[2,3], and the surface and volume magnetic charge densities are defined as is customary ($\sigma = \mathbf{M} \cdot \hat{\mathbf{z}}$, $\rho = \nabla \cdot \mathbf{M}$). Note that the magnetic surface charges arise from the boundary conditions of the magnetization at the top and bottom surfaces of a magnetic thin film, whereas the volume charges arise from the divergence of the magnetization inside the film, i.e. from that of the Néel walls. For the multilayer samples studied here sum of the fields arising from each Co-layer was calculated. The magnetization of the Co layer was chosen to obtain the total magnetic moment of the sample measured by VSM. Because all magnetic moment was attributed to the Co layers, a polarization of the Pt layers could be neglected.

Magnetization pattern from domain pattern measurements

The magnetization pattern (i.e., essentially, $\sigma = \mathbf{M} \cdot \hat{\mathbf{z}}$) corresponding to a domain pattern measurement is found by first discriminating the frequency shift values that are above or below the level of the domain wall center. This yields a binary pattern, which may have artifacts at the center of large domains, where on account of the thickness loss factor the field can dip below the noise level. These artifacts are simple to remove. Subsequently, the pattern is scaled to the measured saturation magnetization, M_{Co} = 653.6 kA/m. The domain wall profiles[5] are embedded in the binary patterns in Fourier space, by replacing the sharp steps with the Fourier transform of a Bloch profile, calculated from A = 16 pJ/m, K_u = 414 kJ/m^3 (obtained from VSM).

Skyrmion Profiles and Dzyaloshinskii-Moriya interaction determination

For the calculation of the skyrmion spin profiles we use the functional

$$w = \sum_i \left[\left(\frac{\partial \boldsymbol{M}}{\partial \tilde{x}_i} \right)^2 - \tilde{\beta} M_z^2 - \boldsymbol{M} \cdot \boldsymbol{H}_{ext} - \frac{1}{2} \boldsymbol{M} \cdot \boldsymbol{H}_d + \boldsymbol{\omega}_D \right] \tag{5}$$

in which the external- and demagnetization fields $\boldsymbol{H}_{ext}$ and $\boldsymbol{H}_d$ have been reduced with $H_D \equiv D^2/A\,K$ (D is the DM interaction coefficient, K the anisotropy energy and A the exchange stiffness). The anisotropy constant is reduced to $\tilde{\beta} \equiv AK/D^2$, and the DM interaction expressed as $\boldsymbol{\omega}_D = -D\left[M_x \frac{\partial \boldsymbol{M_z}}{\partial \tilde{x}} - M_z \frac{\partial \boldsymbol{M_x}}{\partial \tilde{x}} + M_y \frac{\partial \boldsymbol{M_z}}{\partial \tilde{y}} - M_z \frac{\partial \boldsymbol{M_y}}{\partial \tilde{y}}\right]$.

For our finite thickness film $\boldsymbol{H}_d$ is non-local and cannot be replaced with the local approximation $\boldsymbol{H}_d = -\boldsymbol{M}$ for infinitesimally thin- or $\boldsymbol{H}_d = 0$ for infinitely thick media. For a through-thickness homogenous magnetization pattern $\boldsymbol{M}_{Co}$ containing a skyrmion we calculate a constant factor α iteratively from $\alpha_0 \approx \sqrt{\frac{t_{Co}}{t_{Co}+t_{non-mag}}} = 0.522$ such that over the multilayer volume V:

$$\frac{1}{2}\int_V \alpha^2 \boldsymbol{M_{Co}} \cdot \boldsymbol{M_{Co}}\, dv = -\frac{1}{2}\int_V \boldsymbol{M}_{loc.} \cdot \boldsymbol{H}_d\, dv \tag{6}$$

where $\boldsymbol{M}_{loc}$ is the magnetization distribution of the stack of Co layers, i.e. it is equal to M_{Co} inside the Co layers and is set to zero elsewhere in the film. We use this to replace $\boldsymbol{H}_d = -\alpha^2\boldsymbol{M}$ in Eq. (2) and numerically solve the Euler equation resulting[6] from the energy functional (5) assuming cylindrical symmetry.

From the resulting D-dependent skyrmion profiles (Figure 3a of the main text) the z-component of the field can be calculated and compared with measurement by convolution with the tip-calibration function (1). In the example described in the main text, this yields a value of $D = +3.41 \pm 0.01$ mJ/m^2 at the location of the skyrmion.

Additional thin film multilayer systems

In Figure 2 we demonstrate the Halbach magnetization structure in chiral Pt/Co/CoNi/Ni/Pt and Pt/Co/CoNi/Ni/Ag multilayers. For reference, we sputter-deposit achiral Pt/Co/Pt-based multilayers (Fig. 2a), for which $D \approx 0$. At this thickness, the balance of domain wall and magnetostatic energy leads to the stabilization of large domains with about the same domain wall contrast on either side of the film (Figures 2d, g, and corresponding sections j, m).

The $Pt_{1nm}/Co_{0.4nm}/NiCo_{0.4nm}/Ni_{0.4nm}/Pt_{0.4nm}$ multilayer (Fig. 2b) with an expected $D < 0$ yields domains of $\sim$250 nm width. They result in domain contrast of 9.17 Hz at 12.0 ± 0.5 nm (Figures 2e,k). Measuring at the same distance to the opposite side of the multilayer (which amounts to the reverse stack and $D < 0$), shows a contrast of 6.35 Hz (Figures 2h,n). There is thus an amplification of 1.44 or an attenuation to 0.69, respectively, upon going from the bottom to the top side, or vice versa.

A similar observation is made for $Pt_{1nm}/Co_{0.4nm}/NiCo_{0.4nm}/Ni_{0.4nm}/Ag_{0.4nm}$ multilayers (Fig. 2c). They have slightly larger domain size ($\sim$350 nm). Measuring on the top (Ni/Ag-) side results in domain contrast of 17.85 Hz at 12.0 ± 0.5 nm (Figures 2f,l). Measuring at the same distance to the opposite side of the multilayer results in a contrast of 10.54 Hz (Figures 2i, o), so that the amplification (attenuation) factor is 1.69 (0.59).

Note that although the domains are of the order of 100 nm, the film thickness is an order of magnitude smaller, and consequently the amplitude ratio is smaller than the simulation results from Figure 1 in the main text.

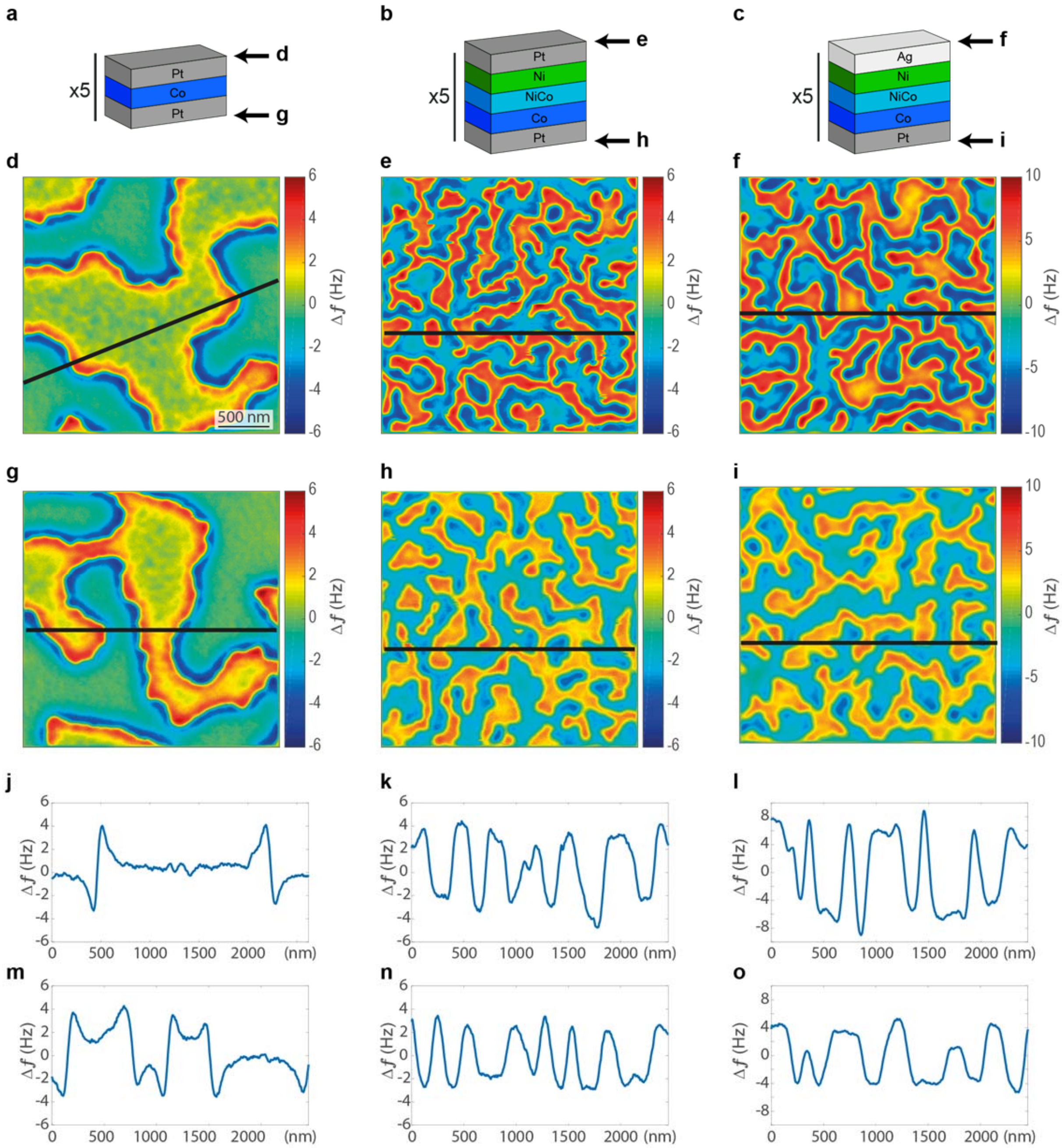

Figure 2: Halbach effect in Pt/Co/CoNi/Ni/X-based multilayer systems. a Construction schematic of the reference achiral Co/Pt multilayer. **b** Schematic of the chiral multilayer with X = Pt. **c** Schematic of the chiral multilayer with X = Ag. **d**-**f** Frequency-shift measurements corresponding to the multilayers **a**-**c**, respectively, at 12±0.5 nm distance to the upper film surface. **g**-**i** Frequency-shift measurements corresponding to the multilayers **a**-**c**, respectively, at 12±0.5 nm distance below the bottom film surface. **j**-**l** Sections across the black lines in **d**-**f**. **m**-**o** Sections across the black lines of **g**-**i**.

References

(1) Hug, H. J.; Stiefel, B.; Schendel, P. J. A. van; Moser, A.; R.Hofer; Martin, S.; Güntherodt, H.-J.; Porthun, S.; Abelmann, L.; Lodder, J. C.; Bochi, G.; O'Handley, R. C.. Quantitative Magnetic Force Microscopy on Perpendicularly Magnetized Samples. *J Appl Phys* **1998**, *83*, 5609–5620.

(2) Bertram, H. N. *Theory of Magnetic Recording*; Cambridge University Press: Cambridge, Great Britain; New York, NY, USA., 1994.

(3) Camras. *Magnetic Recording Handbook*; Springer Science & Business Media, 2012.

(4) Schwenk, J.; Zhao, X.; Bacani, M.; Marioni, M. A.; Romer, S.; Hug, H. J. Bimodal Magnetic Force Microscopy with Capacitive Tip-Sample Distance Control. *Appl. Phys. Lett.* **2015**, *107*, 132407.

(5) Rohart, S.; Thiaville, A. Skyrmion Confinement in Ultrathin Film Nanostructures in the Presence of Dzyaloshinskii-Moriya Interaction. *Phys. Rev. B* **2013**, *88*, 184422.

(6) Bogdanov, A.; Hubert, A. Thermodynamically Stable Magnetic Vortex States in Magnetic Crystals. *J. Magn. Magn. Mater.* **1994**, *138*, 255–269.